

On the Scaling Relations of Disk Galaxies

Riccardo Giovanelli

Dept. of Astronomy, Cornell University,
Space Sciences Bldg., Ithaca, NY 14853, USA
email: rg39@cornell.edu

Abstract. The physical background of scaling laws of disk galaxies is reviewed. The match between analytically derived and observed scaling laws is briefly discussed. Accurate modeling of the fraction of baryons that end populating a disk, and the conversion efficiency of those into stars, remains a challenging task for numerical simulations. The measurement of rotational velocity tends to be made with criteria of convenience rather than through rigorous definition. And yet, the Tully-Fisher and the disk size vs. rotational velocity relations exhibit surprisingly low scatter. Practical recipes (and costs) to optimize the quality of template relations are considered.

Keywords. galaxies: distances and redshifts, galaxies: halos, galaxies: spiral, cosmology: distance scale

1. Introduction

Thirtyfive years have passed since Brent Tully and Rick Fisher advocated the use of the relation between optical luminosity L and 21cm HI linewidth W , previously discovered by Mort Roberts, as a tool to obtain redshift-independent distances of spiral galaxies (Roberts 1969; Tully & Fisher 1977). Since then, the Tully-Fisher relation (hereafter TFR) has been used extensively in the measurement of H_0 and that of deviations from smooth Hubble flow, to distances approaching $z \simeq 0.1$. Over the range of linewidths $W > 100 \text{ km s}^{-1}$, typically used in those applications, the TFR exhibits a tight power-law behavior, where the linewidth is to first order equal to twice the maximum rotational velocity of the disk within galactocentric radii populated with detectable HI, and L a proxy for total mass within that radius. A TFR template will have a slope of between 3 and 4 in $\log L$ vs. $\log W$ and a scatter between 0.14 and 0.18 dex in $\log L$ (0.35 to 0.45 mag), which translates to a distance uncertainty for a single galaxy between 15% and 20%. These values vary somewhat depending mostly on the adopted optical band. The quality of a TFR template, i.e. the accuracy with which it can accurately provide a distance prediction, depends on a variety of parameters, including primarily those pertaining to the selection criteria for membership in the sample used to define that template and the reliability of the corrections applied to the observed quantities. Improvements to that quality should result from a clear understanding of the sources of scatter and of the physical basis of the TFR.

2. Towards a Physical Understanding of the TFR

Take 1: Assume that disk mass and light are exponentials of scale length r_d . The luminosity is then $L \propto r_d^2 I(0)$, where $I(0)$ is the central disk surface brightness. The mass within radius r is $M(< r) \propto r v_{rot}^2$, so if the rotation curve becomes flat due to a DM halo truncated at nr scale lengths, then $M_{tot} \propto nr_d v_{max}^2$ and

$$L_d \propto a v_{max}^4 \quad \text{with} \quad a = (M_d/L_d)^{-2} m_d^2 n^{-2} I(0)^{-2} \quad (2.1)$$

where m_d is the mass fraction of the disk. A rough match for the slope of the TFR is recovered, but much is contained in a .

Take 2. Mo *et al.* (1998) model the DM halo, within which the disk galaxy resides, as a singular isothermal sphere. Then the rotational velocity v_c is the same at all radii, and the mass density at, and the mean density within, radius r are

$$\rho(r) = \frac{v_c^2}{4\pi G r^2} \quad \text{and} \quad \bar{\rho} = \frac{3v_c^2}{4\pi G r^2} \quad (2.2)$$

The critical density of the universe at redshift z is

$$\rho_{crit} = \frac{3H^2(z)}{8\pi G} \quad (2.3)$$

so the radius within which the mean density is $200\rho_{crit}$ is $r_{200} = v_c/10H(z)$ and the mass within r_{200} is

$$M_{halo} = v_c^2 r_{200} / G = v_{200}^3 / 10GH(z); \quad (2.4)$$

Introducing the disk mass M_{disk} and $m_d = M_{disk}/M_{halo}$ we get

$$M_d = \frac{m_d v_{200}^3}{10 G H(z)} \simeq 1.7 \times 10^{11} h^{-1} M_\odot \left(\frac{m_d}{0.05} \right) \left(\frac{v_{200}}{250 \text{ kms}^{-1}} \right)^3 \left[\frac{H(z)}{H_o} \right]^{-1} \quad (2.5)$$

This is starting to look familiar, but:

- halos are not singular isothermal spheres;
- disks' masses are not negligible and they can alter the total density profile;
- we measure disk luminosity, not disk mass;
- we don't measure v_{200} but rather a circular(?) velocity at whatever radius Nature kindly leaves a tracer for us to measure.

Take 3. We thus abandon the singular isothermal sphere model and, still following Mo *et al.* (1998), model the mass density more realistically with the NFW profile:

$$\rho(r) = \frac{\rho_{crit} \delta_o}{(r/r_s)(1+r/r_s)^2} \quad (2.6)$$

where $\delta_o = 4\rho(r_s)/\rho_{crit}$ and $c = r_{200}/r_s$ is the concentration index. The mass within radius r is then

$$M(r) = 4\pi\rho_{crit} \delta_o r_s^3 \left[\frac{1}{1+c(r/r_{200})} - 1 + \ln(1+r/r_{200}) \right], \quad (2.7)$$

the total halo mass is

$$M_{halo} = 4\pi\rho_{crit} \delta_o r_s^3 \left[\ln(1+c) - c/(1+c) \right] \quad (2.8)$$

and the rotation curve is

$$\frac{v(r)}{v_{200}} = \left[\frac{1}{x} \frac{\ln(1+cx) - cx/(1+cx)}{\ln(1+c) - c/(1+c)} \right]^{1/2} \quad (2.9)$$

where $x = r/r_{200}$ and $v_{200} = (GM_{halo}/r_{200})^{1/2}$.

Figure 1 (after Mo *et al.* 1998) shows rotation curves of galaxies having the same disk mass but different combinations of concentration indices, disk mass fractions, spin parameters. The shape of the rotation curve, its maximum value and its value at the virial radius (indicated by the short, thick line at the left of each box), vary widely from each other, illustrating the uncertainty that can be associated with the determination of the

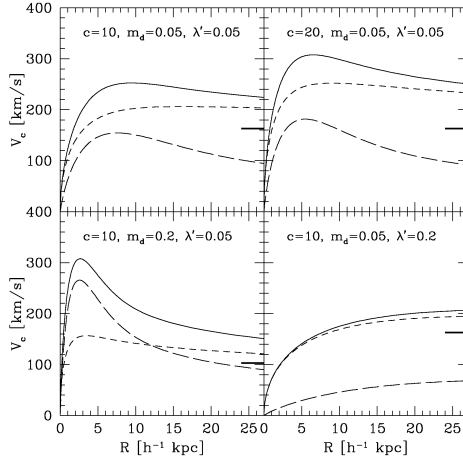


Figure 1. NFH rotation Curves of galaxies having the same disk mass ($5 \times 10^{10} h^{-1} M_{\odot}$) and different combinations of concentration indices, disk mass fractions, spin parameters, as inset within each box. Disk and halo contributions to the rotation curve (solid line) are respectively shown as long-dash and short-dash lines. The thick line on the left of each panel is the circular velocity v_{200} at the virial radius. Note the variance in the shape of the rotation curves and in their amplitudes at any radius (credit: Mo *et al.* 1999).

TFR linewidth parameter. Because now $v_{rot}(r)$ is not constant, it matters at which radius r_{meas} it is measured. It is sensible to measure it at a radius near which the gradient of v_{rot} is small, e.g. the radius within which 80% of the light is produced, or a few disk scale lengths nr_d out (a value of $n \simeq 3$ is often used, and r_{80} is near $3r_d$). The equation for M_d is then modified via a fudge factor which accounts for the shape of V_{rot} and the radius at which it is measured. E.g. if $r_{meas} = 3r_d$, then that fudge factor is $f_v = [v_{rot}(3r_d)/v_{200}]^{-3}$. Finally, to convert the disk mass relation into a TFR look-alike, M_d is divided by a stellar mass-to-luminosity ratio; a star formation efficiency factor ϵ_{sf} is also introduced, which accounts for the fraction of the disk baryon mass which has been converted to stars. Thus:

$$L_d = 1.7 \times 10^{11} h^{-1} M_{\odot} \epsilon_{sf} \left(\frac{m_d}{0.05} \right) \left(\frac{M}{L} \right)_*^{-1} \left[\frac{v_{obs}(3r_d)}{250 \text{ km s}^{-1}} \right]^3 \left[\frac{H(z)}{H_0} \right]^{-1} f_v \quad (2.10)$$

Accurately modeling $m_d \epsilon_{sf} (M/L)_*^{-1}$ is difficult, and so is measuring f_v . Moreover, the value of the rotation curve at $3r_d$ may not be known from the kinematic data. Much progress has been made since Steinmetz & Navarro (1999) in modeling the gastronomy of disks, thanks to increased resolution of numerical simulations and a higher grade of sophistication in treating feedback mechanisms, including adiabatic contraction of the halo (e.g. Governato *et al.* 2007; Piontek & Steinmetz 2011). Generally, simulations recover the slope of the TFR but have problems in reproducing the photometric zero-point. In particular, the stellar mass fraction in hydrodynamical simulations tends to be too high and bulges too large, while galaxies at low z are too gas-poor (Scannapieco *et al.* 2012). Improvements are obtained by forcing a slow-down in the growth of bulges. However, processes of feedback, those affecting ISM structure and metallicity and their effect on star formation take place on scales which are still much smaller than those currently achievable by cosmological simulations. As for f_v , an interesting observational

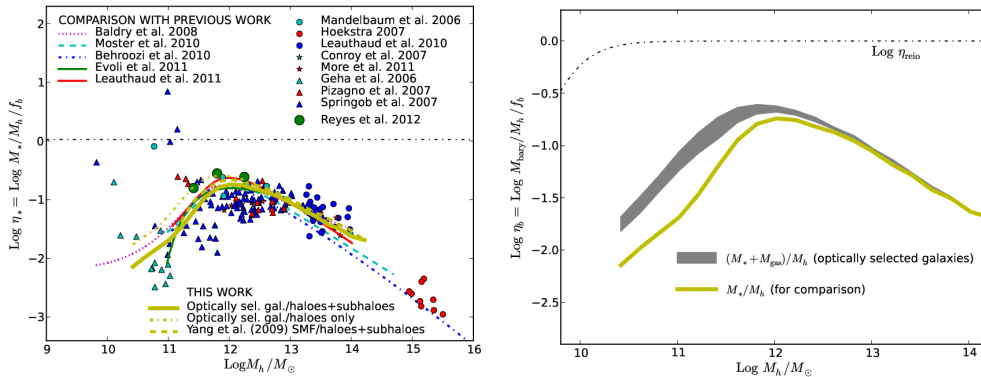


Figure 2. *Left:* Stellar mass as a fraction of the baryon mass within the halo, plotted vs. the halo mass; the baryon mass within the halo is $f_b M_{\text{halo}}$, where f_b is the cosmic baryon fraction. *Right:* The observable baryon mass (stars plus disk ISM) as a fraction of the total baryon mass within the halo (shaded curve). The thin line is the stellar mass fraction, as in the panel to the left (credit: Papastergis *et al.* 2012, reproduced with permission off the American Astronomical Society).

result has recently come to the fore, throwing additional light on equation 2.10, as we see next.

Reyes *et al.* (2012) directly measured averaged f_v , implementing a technique earlier adopted by Seljak (2002). They used the SDSS data base, stacking images of 133,598 disk galaxy images at a mean $z = 0.07$, in three bins of stellar mass. The signature of weak lensing was identified in the stacked images, thus yielding averaged halo masses out to r_{200} . The stellar mass bins were centered respectively at $M_* = 0.6, 2.7$ and $6.5 \times 10^{10} M_\odot$. They could then measure M_{200} and r_{200} , hence v_{200} . From a child catalog of galaxies with resolved rotation curves, they obtained $v_{\text{obs}}(r_{80})$; then the averages of the ratios $v_{\text{obs}}(r_{80})/v_{200}$, respectively for the three stellar mass bins, were found to be 1.27, 1.39 and 1.27. Interestingly, the corresponding stellar masses, as fractions of the total baryon mass $f_b M_{200}$, computed assuming baryons are present with the cosmic abundance within the halo, are 0.15, 0.26 and 0.23 for the three stellar mass bins, where $f_b = 0.169$ is the cosmic baryon mass fraction. Disk galaxies in the three stellar mass bins fall short of converting their baryons into stars by factors of between 4 and 5. This is illustrated graphically in figure 2 (after Papastergis *et al.* 2012). In each panel the abscissa is the halo mass; in the left panel, the ordinate is the ratio of the stellar mass to $f_b M_{200}$. in the right panel, the ordinate is the ratio of the combined baryon mass of stars and cold disk gas to $f_b M_{200}$. The mismatch between the observed baryon mass in disks and that which would be expected if the baryons were present within the halo in the fraction f_b is thought to be mainly due: (a) for low halo masses: to the inability of the halos to hold on to their baryons, which increases with decreasing halo mass; (b) for galaxies near the peak of the curve: likely to the fact that in those systems most baryons are in hot galactic coronae, rather than in disks. The Reyes *et al.* (2012) data are identified by the three circles near the top of the curve in the left panel.

Equation 2.10 and figure 2 summarize our understanding of the physical basis of the TFR. It remains surprising that the variance on the combination of parameters $m_d \epsilon_{sf} (M/L)^{-1} f_v$ is as small as indicated by the TFR observed scatter, and that the baryonic version of the TFR remains a pure power law over 5 orders of magnitude in mass (see Figure 4 and discussion in Section 4).

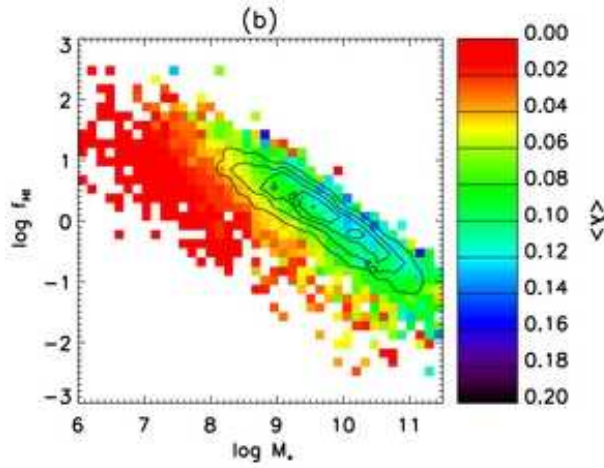


Figure 3. HI gas fraction $f_{HI} = M_{HI}/M_*$ of 7459 ALFALFA survey galaxies plotted against the stellar mass M_* ; shading (color) represents the mean value of the spin parameter λ within each $(\log f_{HI}, \log M_*)$ cell. Cells in the diagram containing more than 20 galaxies fall within the region bounded by contour lines. The typical galaxy used for TFR in cosmic distance studies falls within a few highly populated cells (those within the contour lines) in the diagram with $\log M_* > 10$ and $\log f_{HI} > 0.1$. As Huang *et al.* point out, the mean value of λ remains nearly constant along lines of constant $\log f_{HI}$. See section 3.1 for discussion. (credit: Huang *et al.* 2012. Reproduced with permission from the American Astronomical Society)

3. Understanding Sources of Scatter: the RV Scaling Law

An interesting case study on the sources of scatter is that of the disk size vs. V_{obs} (for short RV) scaling law. Assuming the baryons collapse within the potential well of the halo without altering its density profile, radiating but conserving angular momentum, and settling into a thin, exponential disk of scale length r_d , a reasoning similar to that described in the previous section yields

$$r_d \simeq 8.8h^{-1} \left(\frac{\lambda}{0.05} \right) \left(\frac{j_d}{m_d} \right) \left(\frac{v_c}{250 \text{ km s}^{-1}} \right) \left[\frac{H(z)}{H_0} \right]^{-1} f_c f_R \text{ kpc} \quad (3.1)$$

where λ is the spin parameter of the halo, j_d the fraction of the angular momentum carried by the disk, f_c a fudge factor which depends solely on the concentration index of the NFW halo profile and f_R a factor which depends mainly on the shape of the rotation curve.

An important source of scatter in this relation would appear to be that driven by the variance in λ . N-body simulations show that, over all halos, λ has a log-normal distribution centered near 0.045 with a scatter of 0.22 dex in $\log \lambda$. Thus, it would be expected that the observed scatter of the RV law would be greater than 0.22 dex in $\log r_d$. Yet, the observed scatter is no greater than 0.16 (Courteau *et al.* 2007, Saintonge & Spekkens 2011). The possible explanation of the mismatch is in Figure 14 of Huang *et al.* (2012), reproduced here as figure 3. Using the $\alpha.40$ release of the ALFALFA survey (Haynes *et al.* 2012), Huang *et al.* derive spin parameters of 7459 galaxies using the estimator

$$\lambda = 21.8 \frac{r_d [\text{kpc}]}{V_{rot}^{3/2} [\text{km s}^{-1}]}. \quad (3.2)$$

The inferred values of λ are very coarse, and their dispersion is, as a result, much broader

than the intrinsic one. In a plane of HI gas fraction $f_{HI} = M_{HI}/M_*$ vs. stellar mass M_* , the average value of λ within each cell of that plane is represented by a different degree of shading (color). Cells containing more than 20 galaxies fall within the region bounded by contour lines. The typical galaxy used by the TFR in cosmic distance studies falls within a few highly populated cells (those within the contour lines) of the diagram, stretching along lines of roughly constant HI mass in the region with $\log(M_*/M_\odot) > 9.5$ and higher than average $\log f_{HI}$ for any given M_* . Because the λ estimator used is a ragged one, it is not possible to derive the intrinsic $\log \lambda$ scatter. However, as Huang *et al.* point out, it is apparent in figure 3 that the mean value of λ remains nearly constant along lines of constant M_{HI} . Thus, the typical TFR target galaxies are extracted from a sample with much tighter variance than the HI-selected lot shown in the figure. It appears safe to assume that the scatter in $\log \lambda$ in galaxies of a TFR sample is smaller by at least a factor of 2 than that in any sample representative of the global halo mass function resulting from numerical simulations, estimated to be about 0.22 dex. The less than initially feared impact of λ -scatter on the RV law makes the latter a desirable complement to TFR. Saintonge & Spekkens (2011) find that the scatter of the I-band RV relation can be reduced to ~ 0.11 dex on the linear size parameter, if r_d is replaced with an isophotal radius measured at a large enough galactocentric distance so that the disk is transparent and the isophotal radius requires no correction for opacity. Such an RV relation is comparable in predictive quality with the TFR. Saintonge & Spekkens use a template RV relation using the Cornell SCI data set to derive an estimate of the Hubble parameter: $H_0 = 72 \pm 7 \text{ km s}^{-1} \text{ Mpc}^{-1}$.

4. Ways to Improve Your Scaling Law Template

Significant benefits to a cosmic distances program based on disk galaxy scaling laws can result from wise choices in terms of template sample selection and optimization of photometric and kinematic parameters.

- **Sample Selection: All Sky.** The CMB dipole is due to the peculiar velocity of the Milky Way. It produces an apparent reflex motion, with respect to the observer, of galaxies in shells of progressively increasing radius. Asymptotically, that motion converges both in amplitude and apex direction toward the CMB dipole vector. Convergence is reached at shell radii of ~ 100 Mpc (Giovanelli *et al.* 1998, Dale & Giovanelli 2000). Combined with their clustering properties, an uneven distribution of galaxies in the template sample can produce TFR template relations with an incorrect zero-point, simulating inflating or deflating, Local Group-centered Hubble bubbles.

- **Sample Selection: Basket of Clusters.** Photometric parameters of galaxies, such as inclinations to the line of sight and disk scale lengths, are best measured for relatively nearby objects. Peculiar velocities of galaxies can contribute a measurable fraction of TFR scatter at distances up to $\simeq 100$ Mpc. In the case of a cluster with N measured members, the offset from a template due to the cluster motion can be gauged with an accuracy about \sqrt{N} times better than for a single galaxy. Thus, if the TFR template sample consists of galaxies in clusters, the component of the scatter introduced by each cluster's peculiar velocity is removable. This can be achieved by adding cluster galaxies to the template after their offset from the mean TFR, due to the peculiar velocity of their parent cluster, has been removed. A template relation built from galaxies in a basket of clusters will thus have smaller scatter than one obtained for a field galaxy sample.

- **Photometric Band.** Because a good estimate of the kinematical parameter in the TFR requires that galaxies be sufficiently inclined to the line of sight, corrections to the optical flux for internal extinction are an important source of TFR scatter. This advises

for selecting a photometric band within which internal extinction corrections are small, a concern that needs to be weighed against the requirement that the photometry be as representative as possible of the stellar population. Major TFR surveys of the last two decades chose either R or I optical bands as a compromise between the two requirements. More recently, the wide field coverage of the *Spitzer Space Telescope* archival data in the $3.8 \mu\text{m}$ band has offered the opportunity to build substantial TFR samples for which extinction corrections — very small — and homogeneity of the photometric source offer the possibility of reduced scatter. The recent work of Sorce *et al.* (2012) indicates that, while the reliance in a consistent photometric scale over the whole sky is a definite plus, improvements in TFR scatter by going to the mid-IR are not yet substantial: the scatter of a preliminary $3.8 \mu\text{m}$ template is 0.49 mag, which can be reduced to 0.42 mag after introducing a color correction. Contamination by emission from hot dust and PAHs may play a role in the relatively high scatter of this relation.

As just indicated, a color correction can have an important impact in reducing the TFR scatter. Until recently, large TFR samples were monochromatic. A dependence of the TFR template attributed to morphological type has often been found in monochromatic TFR templates (e.g. figures 3 and 4 of Giovanelli *et al.* 1997): that is in fact a color dependence. Availability of multicolor photometry can thus be a good asset towards building a good scaling relation template.

- **Stellar vs. Baryonic.** In the TFR, disk luminosity is considered a proxy for stellar mass, and the relation becomes significantly noisier for disks with rotational velocities smaller than 50 km s^{-1} . However, the power law character of the TFR is preserved through slower rotators if disk luminosity is replaced with the baryon mass, defined as the sum of the ISM mass, as obtained via the 21cm HI line, and the stellar mass as inferred from the disk luminosity and color. Figure 4 (after McGaugh 2012) shows the

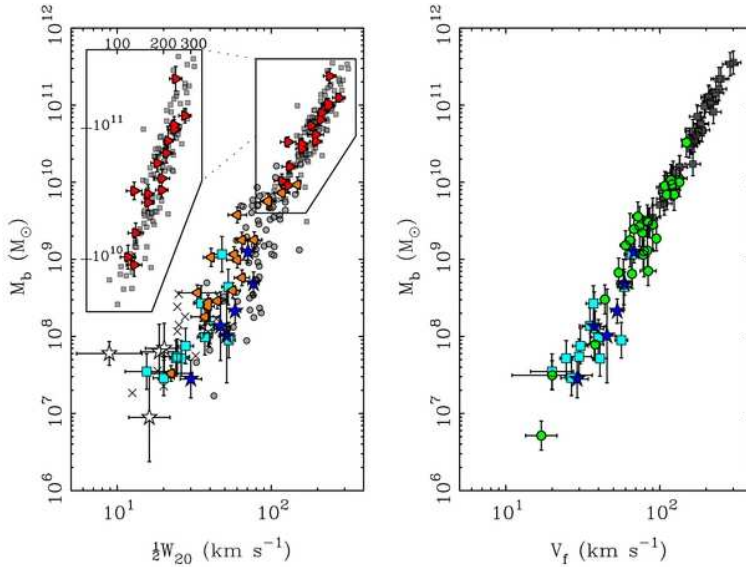


Figure 4. Baryonic mass as a function of half line width (left) and circular velocity as obtained from resolved rotation curves (right). The section of the plot for the high mass end of the relation is overplotted with higher resolution on the left panel. Note (a) the power law extension of the relation all the way to the low mass end and (b) the significant reduction of the scatter when the rotational velocity is extracted from a resolved rotation curve (credit: McGaugh 2012; reproduced with permission from the author and the American Astronomical Society).

baryonic TFR behavior as a single power law to rotational velocities as low as 20 km s^{-1} . The usefulness of this relation can apply to the determination of distances to nearby dwarf systems, as an economical substitute for techniques such as the measurement of the TRGB.

- **Line Widths vs. Resolved Rotation Curves.** The two panels of figure 4 differ in the adoption of the kinematic parameter: the scatter in the baryonic TFR is significantly reduced if the rotational velocity is inferred from a resolved rotation curve (the label V_f indicates that the velocity was measured at a radius at which the rotation curve becomes "flat"). A template that uses single-dish HI line widths is economical, but it can be improved if replaced with $\text{H}\alpha$ rotation curves and, even more so, if HI synthesis maps are available, for the HI can be typically detected to larger galactocentric radii than $\text{H}\alpha$ and therefore provide a better sampling of the large-scale dynamics of the galaxy.

- **The Cost of Reduced Scatter.** Several of the recommendations in this section require more data than does the "basic" TFR. For the added value, there is a cost penalty. Since we live in times of fiscal austerity, it can be useful to quantify the cost of reduced scatter. The more "expensive" observational parameter is the kinematical one. Consider three versions of the latter, more often used, and the operating costs of telescopes needed to obtain them., and see how they would impact a TFR project budget:

- Single dish HI line widths; cost: $\sim \$200 \text{ gal}^{-1}$; feasible sample size: $\sim 10^4$
- $\text{H}\alpha$ rotation curve; cost: $\sim \$2\text{K} \text{ gal}^{-1}$; feasible sample size: $\sim 10^3$
- HI synthesis map; cost: $\sim \$15\text{K} \text{ gal}^{-1}$; feasible sample size: $\sim 10^2$

These are very rough numbers. Perhaps better deals can be had after careful shopping.

- **Invitation to Harvest .** By the way, the ALFALFA HI survey is now complete and nearly half of the extragalactic HI sources are in the public domain. The final catalog will contain more than 30,000 sources, including optical identifications, HI masses and line widths. See Giovanelli *et al.* (2005) and Haynes *et al.* (2011).

This work has been supported by a grant of the U.S. National Science Foundation.

References

- Courteau, S., Dutton, A.A., vanden Bosch, F.C. *et al.* 2007, *ApJ* 671, 203
Dale, D.A. & Giovanelli, R. 2000, in "Cosmic Flows Workshop", S. Courteau & J. Willick (eds.) *ASP-CS* 201, p. 25
Giovanelli, R., Haynes, M.P., Freudling, W. *et al.* 1998, *ApJ (Letters)* 505, L91
Giovanelli, R., Haynes, M.P., Kent, B.R. *et al.* 2005, *AJ* 130, 2598
Governato, F., Willman, B., Mayer, L. *et al.* 2007, *MNRAS* 374, 1479
Haynes, M.P., Giovanelli, R., Martin, A.M. *et al.* 2011, *AJ* 142, 170
Huang, S., Haynes, M.P., Giovanelli, R. *et al.* 2012, *ApJ* 756, 113
McGaugh, S.S. 2012, *AJ* 143, 40
Mo, H.J., Mao, S. & White, S.D.M. 1998, *MNRAS* 319, 336
Papastergis, E., Cattaneo, A., Huang, S. *et al.* 2012 arXiv1208.5229
Piontek, F. & Steinmetz, M. 2011, *MNRAS* 410, 2625
Reyes, R., Mandelbaum, R., Gunn, J.E. *et al.* 2011, arXiv1110.4107
Roberts, M.S. 1969, *AJ* 74, 859
Saintonge, A. & Spekkens, K. 2011 *ApJ* 726, 77
Scannapieco, C., Wadepuhl, M., Parry, O.H. *et al.* 2012 *MNRAS* 423, 1726
Seljak, U. 2002, *MNRAS* 334, 797
Sorce, J.G., Tully, R.B. & Courtois, H.M. 2012, *AJ* 144, 133
Steinmetz, M. & Navarro, J.F. 1999, *ApJ* 513, 555
Tully, R. B. & Fisher, J.R. 1977, *AA* 54, 661